

Solvent-Induced Reversible Spin-Crossover in a 3D Hofmann-Type Coordination Polymer and Unusual Enhancement of the Lattice Cooperativity at the Desolvated State

Dibya Jyoti Mondal, Subhadip Roy, Jyoti Yadav, Matthias Zeller, and Sanjit Konar*



Cite This: <https://dx.doi.org/10.1021/acs.inorgchem.0c02240>



Read Online

ACCESS |



Metrics & More



Article Recommendations



Supporting Information

ABSTRACT: The new 3D Hofmann-type coordination polymer $[\text{Fe}(\text{dpyu})\{\text{Pt}(\text{CN})_4\}] \cdot 9\text{H}_2\text{O}$ [$\text{dpyu} = 1,3\text{-di}(\text{pyridin-4-yl})\text{urea}$] exhibits reversible interchange between two- and one-step spin-crossover behavior, associated with desorption/resorption of lattice water molecules. Solvent water removal also induces an increase of the spin-transition temperature, indicating strong lattice cooperativity, observed for the first time in a 3D Hofmann-type coordination polymer.

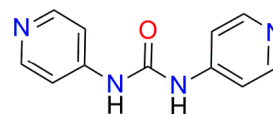
Bistable materials have generated significant interest in the field of materials science.¹ Spin-crossover (SCO) complexes, one of the archetypical bistable materials, generally contain $d^4\text{--}d^7$ metal ions capable of switching between the high-spin (HS) and low-spin (LS) state under an external stimulus (for example, temperature, pressure, light, magnetic field, guest molecules, and so on).² Simultaneously, the SCO phenomenon can also induce remarkable changes in the various material properties ranging from mechanical to optical to magnetic to polarizability, etc., thus paving the way for numerous potential applications such as switching devices, multistitches, and high-order data storage.³

Many SCO complexes have been synthesized over the past decades by varying the nature of ligands, noncoordinating counterions, and solvent molecules, and a wide range of SCO behaviors, including hysteretic, complete, incomplete, abrupt, and gradual one-step and multistep transitions, have been reported.⁴ The results have shown that attaining elastic cooperativity between metal centers through the maximization of intermolecular interactions, such as hydrogen bonding, $\pi \cdots \pi$ stacking, van der Waals, etc., is key to strategically developing functional SCO materials for potential applications.^{2b,5} Another successful strategy involves the design of SCO ion-bearing coordination polymeric networks, where interactions between the spin-transition centers are facilitated by strong coordination bonding.^{5,6} Indeed, a porous SCO coordination polymer featuring fine-tuned host–guest interaction can combine the benefits of the above two strategies to render multipath propagation of elastic interactions throughout the lattice.⁵ In this context, a fascinating platform to obtain differing degrees of cooperativity is offered by the Hofmann-type SCO coordination polymers, where four CN groups from tetracyanometalate bridging ligands occupy the basal positions of $[\text{FeN}_6]$ sites and monodentate or bis-monodentate ligands link the axial positions into 2D or 3D networks.^{2c,4a,5,7} Multistep transitions have been targeted successfully in this type of system via clever modification of the bimetallic interlayer spacing and the generation of inequivalent SCO

sites.^{8,9} The 3D Hofmann-type metal–organic framework reported by Kepert and co-workers, namely, $\text{dpsmePt-}^2/3\text{dpsme} \cdot x\text{EtOH} \cdot y\text{H}_2\text{O}$ ⁸ [where $\text{dpsme} = 4,4'\text{-di}(\text{pyridylthio})\text{methane}$], represents an exemplary case where a unique hysteretic three-step spin transition has been reported. The SCO properties in Hofmann-type coordination polymers are also found to be affected by the guest shape, size, and location, cavity within the host lattice, functional groups present in the guest and host, interaction type and strength, and guest adsorption/desorption processes.^{4a}

In the present study, to construct a Hofmann-type coordination polymer, a bent-flexible pillar ligand, namely, [1,3-di(pyridin-4-yl)urea] (dpyu; Scheme 1), was selected that

Scheme 1. Representation of the dpyu Ligand



is functionalized with a hydrogen-bond-capable urea backbone to promote both internetwork urea \cdots urea synthons as well as urea–solvent (guest) interactions.¹⁰ Thus, a new 3D coordination polymer, $[\text{Fe}(\text{dpyu})\{\text{Pt}(\text{CN})_4\}] \cdot 9\text{H}_2\text{O}$ [$1(\text{Pt}) \cdot 9\text{H}_2\text{O}$], has been synthesized and characterized. The compound exhibits cooperative single-step SCO behavior with a 9 K thermal hysteresis loop ($T_{1/2\uparrow} = 190$ K and $T_{1/2\downarrow} = 181$ K). Remarkably, a two-step SCO behavior has been observed and the spin-transition temperature increases upon desorption of guest solvent water molecules at the

Received: July 28, 2020

expense of hysteresis, signifying an improvement of the lattice cooperativity. This phenomenon is unprecedented in 3D Hofmann-type coordination polymers. The resorption of water molecules reestablishes the one-step SCO behavior.

Light-yellow hexagonal-shaped single crystals of $\mathbf{1}(\text{Pt})\cdot 9\text{H}_2\text{O}$ were obtained using slow reactant diffusion by layering an aqueous solution of $\text{Fe}(\text{ClO}_4)_2\cdot 6\text{H}_2\text{O}$ onto an ethanolic solution of the dpyu ligand and $\text{K}_2[\text{Pt}(\text{CN})_4]$ (see the Supporting Information for details).

The 100 K single-crystal data of $\mathbf{1}(\text{Pt})\cdot 9\text{H}_2\text{O}$ (see the Supporting Information for details) reveal that the compound is a typical 3D Hofmann-type coordination polymer.^{4a} It crystallizes in the orthorhombic crystal system with the space group $Pm\bar{m}m$.

The asymmetric unit of $\mathbf{1}(\text{Pt})\cdot 9\text{H}_2\text{O}$ features one iron(II) center, one independent platinum atom with a half-disordered ligand, a CN fragment, and a lattice water molecule (Figure 1a). The geometry of the iron(II) atom is slightly distorted from a regular octahedron. The four equatorial positions are coordinated to the symmetry-equivalent cyanide nitrogen atoms of $[\text{Pt}(\text{CN})_4]^{2-}$ fragments, and the two axial sites are taken up by the nitrogen atoms of bridging dipyrindyl urea ligands (Figure 1b). The dpyu ligand and resolved solvate water molecules exhibit systematic symmetry-imposed disorder (see Figure S1 for details) that is partially static by a whole rotation of the entire ligand and partially dynamic by slight offsets of the ligands from a crystallographic mirror plane, induced by hydrogen bonding to the symmetry-disordered water molecule [Figure 1c; established by thermogravimetric analysis (TGA) measurements]. The lattice void space that accounts for about half the lattice volume (at least 46%; see Figure 1d,e and the Supporting Information) contains an additional eight unresolved water solvate molecules. Further structural details can be found in the Supporting Information.

Upon an increase of the temperature, the symmetry-induced disorder, large void space, and pronounced liberation of the ligands lead to a substantial drop in data quality, and no useful numerical data related to, e.g., spin states at the iron center, can be extracted anymore. The general structure is, however, maintained [also evidenced by powder X-ray diffraction (PXRD)]. It is worth pointing out that the water molecule hydrogen bonded to the urea fragment at 100 K is not resolved at 220 K anymore, indicating that the $\text{O}-\text{H}_{\text{urea}}$ hydrogen bonds are broken at this temperature or become highly fluxional.

To investigate the SCO properties of the framework compound, variable-temperature magnetic susceptibility data of $\mathbf{1}(\text{Pt})\cdot 9\text{H}_2\text{O}$ (powdered sample prepared by grinding the single crystals) were recorded in the temperature range of 2–300 K in both warming and cooling modes with a rate of 3 K min^{-1} (Figure 2). The phase purity of the bulk sample was confirmed by the agreement of the patterns from PXRD with the single-crystal structure data (Figure S8). At 300 K, the value of $\chi_{\text{M}}T$ (3.40 $\text{cm}^3 \text{K mol}^{-1}$) suggests a HS iron(II) state.

Upon cooling, this value remains almost constant up to 204 K, but upon further cooling, it abruptly drops until it reaches, at 150 K, a value of 2.09 $\text{cm}^3 \text{K mol}^{-1}$, which coincides with the $3/5$ fraction of the HS state to the LS site (HS0.6LS0.4). This confirms the one-step incomplete SCO process with critical temperatures $T_{1/2\uparrow} = 190 \text{ K}$ and $T_{1/2\downarrow} = 181 \text{ K}$ in the heating and cooling modes, respectively, with a pronounced hysteresis loop around 9 K due to the strong cooperativity.

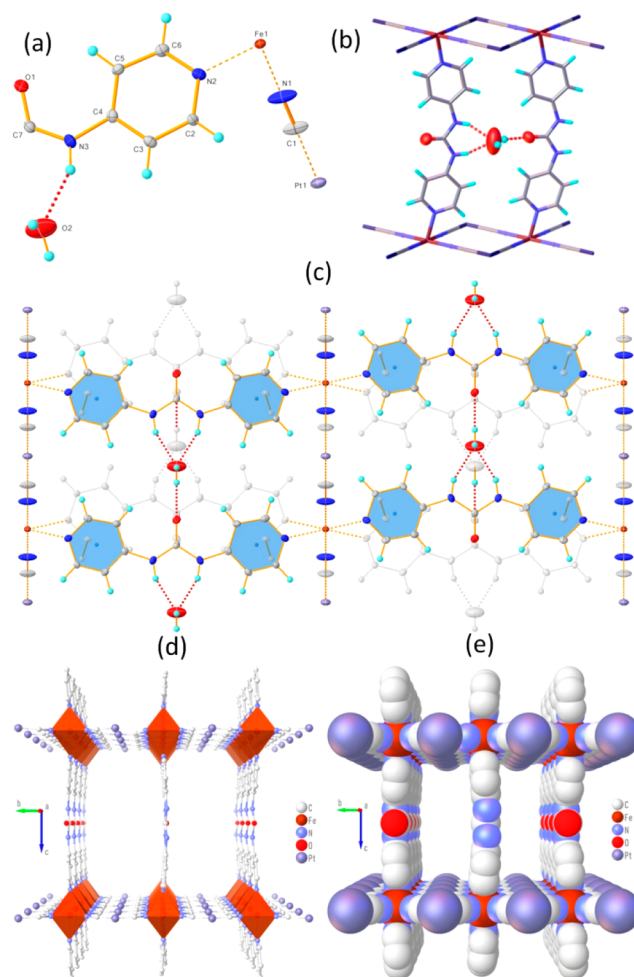


Figure 1. (a) Asymmetric unit of the compound with an atom numbering scheme. (b) View of the framework along the ac plane (only one of four symmetry-equivalent disordered components is shown). (c) Propagation of the network architecture: one ladder down and another ladder up on the other side (alternative disordered components are marked gray). Only the one crystallographically derived water molecule is shown. (d) Perspective view of the network along the a axis without solvent. A total of 46% of the cell is solvent-accessible through the large channel visible here. (e) Space-filling perspective view of the network along the a axis without solvent.

With a further decrease in the temperature, the $\chi_{\text{M}}T$ value gradually drops in a very gradual fashion to a certain level until it reaches 1.95 $\text{cm}^3 \text{K mol}^{-1}$ at ca. 125 K. It then decreases again more rapidly because of zero-field splitting for the rest of the HS iron(II) species.^{11,12} Differential scanning calorimetry (DSC) measurement was performed in the cooling and heating modes (Figure S4). The heat flow (mW) versus T plot shows two well-distinguished peaks in the cooling and heating modes and reflects the changes in the slope of $\chi_{\text{M}}T$ versus T of $\mathbf{1}(\text{Pt})\cdot 9\text{H}_2\text{O}$. The observed critical temperature values ($T_{1/2\downarrow} = 185 \text{ K}$ and $T_{1/2\uparrow} = 198 \text{ K}$) are in agreement with the $T_{1/2}$ values from the magnetic data. The average enthalpy and entropy changes in the cooling (exothermic) and heating (endothermic) modes are $\Delta H = 7.11 \text{ kJ mol}^{-1}$ and $\Delta S = 36.32 \text{ J mol}^{-1} \text{K}^{-1}$, consistent with the values typically displayed by the 3D Hofmann SCO compounds.¹³

To explore the effect of guest molecules on the SCO behavior from the viewpoint of host–guest chemistry, we

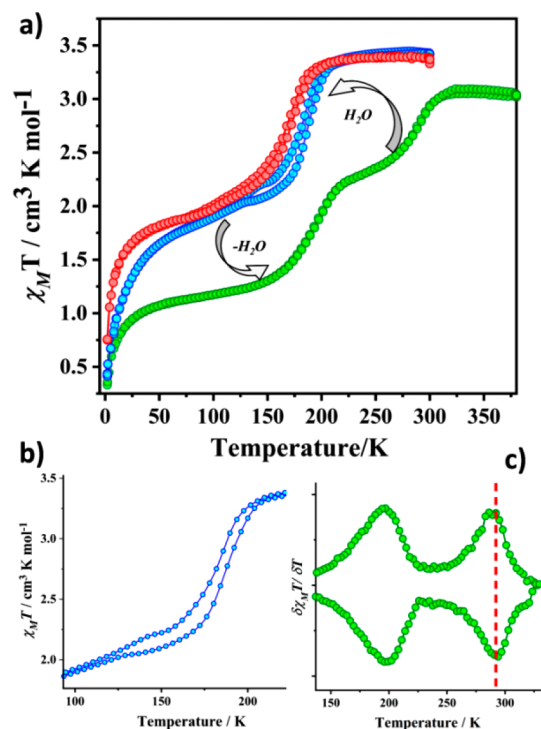


Figure 2. (a) Variable-temperature $\chi_M T$ of $\text{I(Pt)}\cdot 9\text{H}_2\text{O}$: blue, freshly prepared crystalline sample; green, desolvated sample; red, resolvated sample. (b) Hysteresis loop in solvated $\text{I(Pt)}\cdot 9\text{H}_2\text{O}$. (c) Derivative graph of the desolvated sample, where the red dashed line indicates the room temperature spin-state transition.

investigated desorption of the solvent molecules upon heating of the hydrated polycrystalline sample $\text{I(Pt)}\cdot 9\text{H}_2\text{O}$ at 540 K according to TGA (Figure S5). Using the desolvated material, we measured the temperature dependence of $\chi_M T$ in the range of 380–2 K, revealing a two-step transition in the form of $2/3$ and $1/3$ HS states (Figure 2a). At 380 K, the $\chi_M T$ value of I(Pt) is equal to $3.06 \text{ cm}^3 \text{ K mol}^{-1}$, indicating a HS iron(II) center, which is sustained down to 316 K upon cooling. At 248 K, the $\chi_M T$ value drops in a first step to $2.48 \text{ cm}^3 \text{ K mol}^{-1}$ and in a second step to $1.25 \text{ cm}^3 \text{ K mol}^{-1}$ at 143 K. Below this temperature, $\chi_M T$ decreases further, presumably because of zero-field splitting of the HS iron(II) fraction. As per the first-order derivative plot of $\chi_M T$ versus T (Figure 2c), the first and second step transition temperatures $T_{1/2}$ are 292 and 195 K, respectively. The heating loop follows the same path, without any hysteresis, and represents an incomplete spin-conversion state of the iron(II) sites to LS. The first spin-state switching is at room temperature, which is an important property of any SCO material for practical application purposes (Figure S6). In the absence of a single-crystal X-ray structure because of the partial degradation of crystallinity with dehydration, it was not possible to establish a magnetostructural correlation. However, the phenomenon of two-step SCO behavior with an increase of the spin-transition temperature may be tentatively attributed to the removal of elastic lattice frustration from the guests and host–guest interactions, which compete with host–host interactions.¹⁴ Moreover, upon desorption, the $\text{H}_2\text{O}\cdots\text{urea}$ hydrogen-bonding interactions, which are unfavorable for the HS state because of increased electron density to the iron(II) sites, are eliminated. Consequently, elimination of the solvate water molecules might favor the HS state over the LS state.¹⁵

To capture the overall prospects of structural changes, variable-temperature synchrotron PXRD was employed, revealing the single-phase nature across the spin-state transition range. The shifts in the Bragg reflections correlate well with the temperature dependence of the molar magnetic susceptibility data of the solvated complex and its solvent-free form (Figure 3).

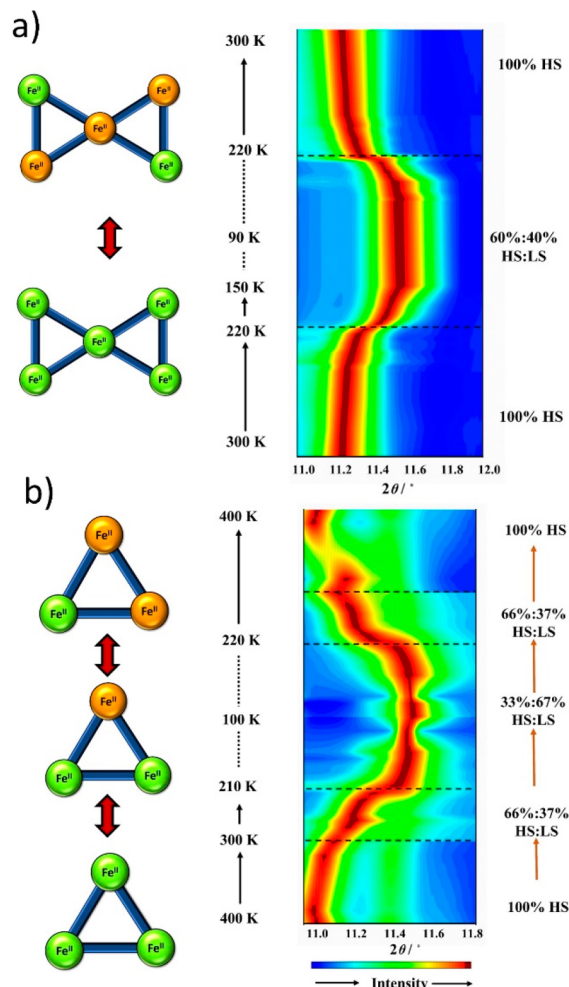


Figure 3. Variable-temperature synchrotron PXRD peak evolution over the range of $11.0\text{--}12.0^\circ$ and schematic graphical diagrams of the iron(II) sites drawn as circles (orange = LS and green = HS): solvated complex $\text{I(Pt)}\cdot 9\text{H}_2\text{O}$ (a); desolvated complex I(Pt) (b).

Furthermore, variable-temperature Raman spectroscopy¹⁴ was performed at three different temperatures to gain some insight into the vibrational details of the HS and LS states of the solvated and desolvated complexes as well as to check retention of the structural framework after solvent water removal (Figure S7). Most importantly, in the Raman spectrum, for the CN vibrational mode, the wavenumber decreases with an increase in the temperature due to a decrease in the CN bond length (strength) from the LS to HS state. The solvated complex exhibits well-resolved doublet peaks at 2187 and 2205 cm^{-1} at 80 K (LS) corresponding to the symmetric and asymmetric stretching modes of the cyanide vibration, respectively, and a prominent band at 2201 cm^{-1} representing the symmetric cyanide stretch at both 250 and 400 K (HS). Similarly, for the desolvated complex, doublet

peaks are observed at 2193 and 2206 cm^{-1} for the $^{2/3}$ LS state (80 K) and at 2190 and 2203 cm^{-1} for the $^{1/3}$ LS state (250 K). A shoulder band appears at 2199 cm^{-1} in the HS state (400 K).¹⁴ Interestingly, the SCO compound also features reversible guest exchange multifunctional properties because the single-step SCO behavior can be recovered when the desorbed sample is resorbed with water molecules. The parent framework is robust toward repeated solvation and desolvation, as evidenced by the PXRD pattern (Figure S8).

In summary, a new 3D Hofmann-type coordination polymer of the formula $[\text{Fe}(\text{dpyu})\{\text{Pt}(\text{CN})_4\}] \cdot 9\text{H}_2\text{O}$ [where dpyu = 1,3-di(pyridin-4-yl)urea] with single-step hysteric SCO behavior has been reported. Although the hysteresis loop is lost, a two-step SCO behavior has been observed and the spin-transition temperature is increased upon desorption of guest solvent water molecules. This is in stark contrast to what is typically observed in 3D Hofmann-type coordination polymers containing guest solvent molecules, where the cooperativity is less pronounced in the desolvated phase because of removal of the host–guest hydrogen-bonding interactions. The rare phenomenon that guest removal positively impacts the lattice cooperativity in this 3D Hoffman-type coordination polymer can be roughly ascribed to the elimination of elastic frustration and host–guest interactions resulting in the proliferation of host–host interactions. The present investigation also revealed reversible guest exchange properties by recovering the one-step spin transition of the complex through resolvation of the desolvated analogue. This endows the host system with a sensory function. Overall, such a compound holds the potential to be an excellent candidate for a futuristic switchable molecular material.

■ ASSOCIATED CONTENT

SI Supporting Information

The Supporting Information is available free of charge at <https://pubs.acs.org/doi/10.1021/acs.inorgchem.0c02240>.

Experimental information, syntheses, PXRD, Fourier transform infrared, magnetic and calorimetric measurement data, Raman spectra, and crystal data and refinement details (PDF)

Accession Codes

CCDC 2012230 contains the supplementary crystallographic data for this paper. These data can be obtained free of charge via www.ccdc.cam.ac.uk/data_request/cif, or by emailing data_request@ccdc.cam.ac.uk, or by contacting The Cambridge Crystallographic Data Centre, 12 Union Road, Cambridge CB2 1EZ, UK; fax: +44 1223 336033.

■ AUTHOR INFORMATION

Corresponding Author

Sanjit Konar – Department of Chemistry, Indian Institute of Science Education and Research (IISER) Bhopal, Bhauri, Bhopal 462066, India; orcid.org/0000-0002-1584-6258; Phone: +91-755-2691313; Email: skonar@iiserb.ac.in; Fax: +91-755-2692392

Authors

Dibya Jyoti Mondal – Department of Chemistry, Indian Institute of Science Education and Research (IISER) Bhopal, Bhauri, Bhopal 462066, India

Subhadip Roy – Department of Chemistry, Indian Institute of Science Education and Research (IISER) Bhopal, Bhauri,

Bhopal 462066, India; Department of Chemistry, The ICFAI University Tripura, Mohanpur, Agartala, Tripura 799210, India; orcid.org/0000-0002-0097-6113

Jyoti Yadav – Department of Chemistry, Indian Institute of Science Education and Research (IISER) Bhopal, Bhauri, Bhopal 462066, India

Matthias Zeller – Department of Chemistry, Purdue University, West Lafayette, Indiana 47907, United States; orcid.org/0000-0002-3305-852X

Complete contact information is available at:

<https://pubs.acs.org/10.1021/acs.inorgchem.0c02240>

Notes

The authors declare no competing financial interest.

■ ACKNOWLEDGMENTS

This work was supported by Science and Engineering Research Board (Project SERB/CRG/2018/000072), Government of India. D.J.M. thanks CSIR, India, for a fellowship, IISER Bhopal for instrumentation facilities, RRCAT-Indore, DAE, Government of India, for the synchrotron radiation source at Beamline-12, UGC–DAE Consortium for Scientific Research, Indore for DSC analysis, and also Dr. Surajit Saha, Department of Physics, IISER Bhopal, for Raman spectroscopy.

■ REFERENCES

- (1) Peng, Y.-Y.; Wu, S.-G.; Chen, Y.-C.; Liu, W.; Huang, G.-Z.; Ni, Z.-P.; Tong, M.-L. Asymmetric seven-/eight-step spin-crossover in a three-dimensional Hofmann-type metal–organic framework. *Inorg. Chem. Front.* **2020**, *7*, 1685–1690.
- (2) (a) Halcrow, M. A. Iron (II) complexes of 2, 6-di (pyrazol-1-yl) pyridines—A versatile system for spin-crossover research. *Coord. Chem. Rev.* **2009**, *253*, 2493–2514. (b) Halcrow, M. A. *Spin-crossover materials: properties and applications*; John Wiley & Sons, 2013. (c) Li, J.-Y.; Ni, Z.-P.; Yan, Z.; Zhang, Z.-M.; Chen, Y.-C.; Liu, W.; Tong, M.-L. Cyanide-bridged bimetallic 3D Hoffman-like coordination polymers with tunable magnetic behaviour. *CrystEngComm* **2014**, *16* (28), 6444–6449. (d) Meng, Y.; Dong, Y.-J.; Yan, Z.; Chen, Y.-C.; Song, X.-W.; Li, Q.-W.; Zhang, C.-L.; Ni, Z.-P.; Tong, M.-L. A New Porous Three-Dimensional Iron (II) Coordination Polymer with Solvent-Induced Reversible Spin-Crossover Behavior. *Cryst. Growth Des.* **2018**, *18*, 5214–5219. (e) Sato, O. Dynamic molecular crystals with switchable physical properties. *Nat. Chem.* **2016**, *8*, 644–656.
- (3) (a) Kahn, O.; Martinez, C. J. Spin-transition polymers: from molecular materials toward memory devices. *Science* **1998**, *279*, 44–48. (b) Halcrow, M. A. Structure: function relationships in molecular spin-crossover complexes. *Chem. Soc. Rev.* **2011**, *40*, 4119–4142.
- (4) (a) Ni, Z.-P.; Liu, J.-L.; Hoque, M. N.; Liu, W.; Li, J.-Y.; Chen, Y.-C.; Tong, M.-L. Recent advances in guest effects on spin-crossover behavior in Hofmann-type metal–organic frameworks. *Coord. Chem. Rev.* **2017**, *335*, 28–43. (b) Zhang, C.-J.; Lian, K.-T.; Huang, G.-Z.; Bala, S.; Ni, Z.-P.; Tong, M.-L. Hysteretic four-step spin-crossover in a 3D Hofmann-type metal–organic framework with aromatic guest. *Chem. Commun.* **2019**, *55*, 11033–11036.
- (5) Li, J.-Y.; He, C.-T.; Chen, Y.-C.; Zhang, Z.-M.; Liu, W.; Ni, Z.-P.; Tong, M.-L. Tunable cooperativity in a spin-crossover Hoffman-like metal–organic framework material by aromatic guests. *J. Mater. Chem. C* **2015**, *3*, 7830–7835.
- (6) Kahn, O.; Codjovi, E.; Garcia, Y.; van Koningsbruggen, P. J.; Lapouyade, R.; Sommier, L. In *Molecule-Based Magnetic Materials*; ACS Symposium Series; Turnbull, M. M., Sugimoto, T., Thompson, L. K., Edd, American Chemical Society, 1996; Vol. 644, p 298.
- (7) (a) Liu, W.; Wang, L.; Su, Y.-J.; Chen, Y.-C.; Tucek, J.; Zboril, R.; Ni, Z.-P.; Tong, M.-L. Hysteretic Spin Crossover in Two-Dimensional (2D) Hofmann-Type Coordination Polymers. *Inorg. Chem.* **2015**, *54*, 8711–8716. (b) Delgado, T.; Meneses-Sánchez, M.;

Piñero-López, L.; Bartual-Murgui, C.; Muñoz, M. C.; Real, J. A. Thermo- and photo-modulation of exciplex fluorescence in a 3D spin crossover Hofmann-type coordination polymer. *Chem. Sci.* **2018**, *9*, 8446–8452. (c) Valverde-Muñoz, F. J.; Muñoz, M. C.; Ferrer, S.; Bartual-Murgui, C.; Real, J. A. Switchable Spin-Crossover Hofmann-Type 3D Coordination Polymers Based on Tri- and Tetra-topic Ligands. *Inorg. Chem.* **2018**, *57*, 12195–12205.

(8) Sciortino, N. F.; Scherl-Gruenwald, K. R.; Chastanet, G.; Halder, G. J.; Chapman, K. W.; Létard, J. F.; Kepert, C. J. Hysteretic Three-Step Spin Crossover in a Thermo- and Photochromic 3D Pillared Hofmann-type Metal–Organic Framework. *Angew. Chem.* **2012**, *124*, 10301–10305.

(9) Liu, W.; Peng, Y. Y.; Wu, S. G.; Chen, Y. C.; Hoque, M. N.; Ni, Z. P.; Chen, X. M.; Tong, M. L. Guest-Switchable Multi-Step Spin Transitions in an Amine-Functionalized Metal–Organic Framework. *Angew. Chem.* **2017**, *129*, 15178–15182.

(10) Banerjee, S.; Adarsh, N.; Dastidar, P. Solvent-driven structural diversities in ZnII coordination polymers and complexes derived from bis-pyridyl ligands equipped with a hydrogen-bond-capable urea backbone. *Cryst. Growth Des.* **2012**, *12*, 6061–6067.

(11) Halder, G. J.; Chapman, K. W.; Neville, S. M.; Moubaraki, B.; Murray, K. S.; Letard, J.-F.; Kepert, C. J. Elucidating the mechanism of a two-step spin transition in a nanoporous metal–organic framework. *J. Am. Chem. Soc.* **2008**, *130*, 17552–17562.

(12) Gütlich, P.; Gaspar, A. B.; Garcia, Y. Spin state switching in iron coordination compounds. *Beilstein J. Org. Chem.* **2013**, *9*, 342–391.

(13) (a) Muñoz, M. C.; Real, J. A. Thermo-, piezo-, photo- and chemo-switchable spin crossover iron (II)-metallocyanate based coordination polymers. *Coord. Chem. Rev.* **2011**, *255*, 2068–2093.

(b) Piñero-López, L. a.; Valverde-Muñoz, F. J.; Seredyuk, M.; Muñoz, M. C.; Haukka, M.; Real, J. A. Guest Induced Strong Cooperative One- and Two-Step Spin Transitions in Highly Porous Iron (II) Hofmann-Type Metal–Organic Frameworks. *Inorg. Chem.* **2017**, *56*, 7038–7047.

(14) Zenere, K. A.; Duyker, S. G.; Trzop, E.; Collet, E.; Chan, B.; Doheny, P. W.; Kepert, C. J.; Neville, S. M. Increasing spin crossover cooperativity in 2D Hofmann-type materials with guest molecule removal. *Chem. Sci.* **2018**, *9*, 5623–5629.

(15) Sciortino, N. F.; Ragon, F.; Zenere, K. A.; Southon, P. D.; Halder, G. J.; Chapman, K. W.; Piñero-López, L.; Real, J. A.; Kepert, C. J.; Neville, S. M. Exploiting pressure to induce a “guest-blocked” spin transition in a framework material. *Inorg. Chem.* **2016**, *55*, 10490–10498.